ity. The transition could thus be accompanied by phase separation between iron-rich HS and magnesium-rich LS ferropericlases. This could explain x-ray diffraction observations suggesting a breakdown of ferropericlase (*24*), which were observed in the same pressure range as our spin transition.

The observed transitions indicate that the lower mantle would be segregated into two different layers characterized by different iron partitioning between perovskite and ferropericlase. The transition pressures are consistent with the depths at which lower mantle layering has been proposed (*1*) and provide a mineral physics basis for an Earth's lower mantle made of two distinct layers. Moreover, observations that the iron-free olivine (forsterite) is more viscous than iron-bearing phases (*25, 26*) imply that, similarly, an iron-free perovskite is likely to be more viscous than an iron-rich one. This idea is also corroborated by the fact that viscosity scales in many materials (*27*) with T/T_m (the ratio of temperature to melting temperature) and that the melting point of an iron-free perovskite is much higher than that of an iron-bearing one (*28, 29*). In that sense, because perovskite is the major lower-mantle phase, the transition could have a fairly strong rheological signature as inferred from geophysical observations (*30*) and could affect the geodynamics in the lowermost mantle. Further studies could constrain geodynamical interpretations (*2, 3*) of the seismic observations and could enable quantification of the effect of such a viscous layer on the dynamics of plumes. Note that such a layering model requires no isolated convection cells, because the chemistry of the two layers is reversible as a function of depth (the transition is reversible upon decompression); uplifted materials will recover the partitioning properties of the top layer.

Iron-free perovskite is stable to very high pressures and temperatures. It was speculated that the breakdown of iron-bearing perovskite (*6*) at the core-mantle boundary (CMB) was responsible for the chemical heterogeneities observed in the D'' layer. We suggest, however, that the iron-free end member is the one that is most likely to be present at those depths, and that the interaction of iron-rich ferropericlase with the liquid outer core should instead be taken into consideration. Geodynamical modeling of this lowermost layer could contribute to our understanding of core-mantle interactions because dominant iron-depleted perovskite could create an electrically, thermally (*31*), and rheologically insulating lid above the CMB.

References and Notes

1. R. van der Hilst, S. Kárason, *Science* **283**, 1885 (1999).
2. T. Lay, Q. Williams, E. J. Garnero, *Nature* **392**, 461 (1998).
3. L. H. Kellogg, B. H. Hager, R. D. van der Hilst, *Science* **283**, 1881 (1999).
4. E. Knittle, R. Jeanloz, *Science* **235**, 668 (1987).
5. S. E. Kesson, J. D. Fitz Gerald, J. M. Shelly, *Nature* **393**, 253 (1998).
6. G. Serghiou, A. Zerr, R. Boehler, *Science* **280**, 2093 (1998).
7. G. Fiquet *et al*., *Geophys. Res. Lett.* **27**, 21 (2000).
8. D. Andrault, *J. Geophys. Res.* **106**, 2079 (2001).
9. S.-H. Shim, T. S. Duffy, G. Shen, *Science* **292**, 2437 (2001).
10. D. M. Shermann, *J. Geophys. Res.* **96**, 14299 (1991).
11. J. Brodholt, unpublished data.
12. R. E. Cohen, I. I. Mazin, D. G. Isaak, *Science* **275**, 654 (1997).
13. The sample $(Mg_{0.83}Fe_{0.17})O$ was prepared by annealing of a mixture of MgO and Fe_2O_3 maintained at 1673 K for 24 hours under a controlled oxygen fugacity between 10^{-9} and 10^{-11} atm. These samples were characterized by x-ray diffraction and shown to be pure ferropericlase.
14. See supporting data on *Science* Online.
15. G. Peng *et al*., *Appl. Phys. Lett.* **65**, 2527 (1994).
16. F. M. F. de Groot *et al*., *Phys. Rev. B* **51**, 1045 (1995).
17. X. Wang *et al*., *Phys. Rev. B* **56**, 4553 (1997).
18. J.-P. Rueff *et al*., *Phys. Rev. Lett.* **82**, 3284 (1999).
19. J. Badro *et al*., *Phys. Rev. Lett.* **83**, 4101 (1999).
20. J.-P. Rueff *et al*., *Phys. Rev. B* **60**, 14510 (1999).
21. F. Sette *et al*., *Phys. Rev. Lett.* **75**, 850 (1995).
22. V. Malavergne, F. Guyot, Y. Wang, I. Martinez, *Earth Planet. Sci. Lett.* **146**, 499 (1997).
23. The critical parameter for this type of transition is density; in the absence of structural phase transitions, the effect of temperature is to increase the transition pressure to compensate for the thermal expansion. It is therefore not possible to express precisely the transition pressures in terms of depths within Earth, because the thermal expansion coefficient at those pressures is not known.
24. L. Dubrovinsky *et al*., *Eur. J. Mineral.* **13**, 857 (2001).
25. W. B. Durham, C. Goetze, *J. Geophys. Res.* **82**, 5737 (1977).
26. W. B. Durham, C. Froideveaux, O. Jaoul, *Phys. Earth Planet. Inter.* **19**, 263 (1979).
27. J. Weertman, J. R. Weertman, *Annu. Rev. Geophys.* **3**, 293 (1975).
28. P. E. van Keken, D. A. Yuen, A. P. van den Berg, *J. Geophys. Res.* **100**, 15233 (1995).
29. A. Zerr, R. Boehler, *Science* **262**, 553 (1993).
30. V. Corrieu, C. Thoraval, Y. Ricard, *Geophys. J. Int.* **120**, 516 (1995).
31. LS ferropericlase is a much better radiative thermal conductor than HS ferropericlase (*10*) because it is transparent to thermal radiation in the near-infrared.

Supporting Online Material

www.sciencemag.org/cgi/content/full/1081311/DC1
SOM Text
Fig. S1
References

9 December 2002; accepted 25 March 2003
Published online 3 April 2003;
10.1126/science.1081311
Include this information when citing this paper.

Diverse Plant and Animal Genetic Records from Holocene and Pleistocene Sediments

Eske Willerslev,[1]* Anders J. Hansen,[1]*† Jonas Binladen,[1] Tina B. Brand,[1] M. Thomas P. Gilbert,[2] Beth Shapiro,[2] Michael Bunce,[2] Carsten Wiuf,[3] David A. Gilichinsky,[4] Alan Cooper[2]

Genetic analyses of permafrost and temperate sediments reveal that plant and animal DNA may be preserved for long periods, even in the absence of obvious macrofossils. In Siberia, five permafrost cores ranging from 400,000 to 10,000 years old contained at least 19 different plant taxa, including the oldest authenticated ancient DNA sequences known, and megafaunal sequences including mammoth, bison, and horse. The genetic data record a number of dramatic changes in the taxonomic diversity and composition of Beringian vegetation and fauna. Temperate cave sediments in New Zealand also yielded DNA sequences of extinct biota, including two species of ratite moa, and 29 plant taxa characteristic of the prehuman environment. Therefore, many sedimentary deposits may contain unique, and widespread, genetic records of paleoenvironments.

Most authenticated ancient DNA studies (*1*) have analyzed hard or soft tissue remains of flora and fauna from the late Pleistocene [~100 to 10 ky (thousand years)] or Holocene (past 10 ky). Preserved genetic information has provided unique insights into many evolutionary and ecological processes (*2–6*) and also provides an important test of methods for reconstructing past events (*7–9*). However, a broader utility for ancient DNA studies has been prevented by experimental difficulties (*1*, *10*) and the rarity of suitable fossilization. Even in areas with excellent ancient DNA preservation and large numbers of specimens, such as Beringia (the late Pleistocene ice-free refugium that stretched from northeast Siberia across the exposed Bering land bridge to western Canada), it has been possible to obtain only limited paleoenvironmental views (*3*). Consequently, we exam-

[1]Department of Evolutionary Biology, Zoological Institute, University of Copenhagen, Universitetsparken 15, Denmark DK-2100 Ø. [2]Henry Wellcome Ancient Biomolecules Centre, Department of Zoology, University of Oxford, Oxford OX1 3PS, UK. [3]Department of Statistics, University of Oxford, 1 South Parks Road, Oxford OX1 3TG, UK. [4]Soil Cryology Laboratory, Institute for PhysicoChemical and Biological Problems in Soil Science, Russian Academy of Sciences, 142290, Pushchino, Moscow Region, Russia.

*These authors contributed equally to this work.
†To whom correspondence should be addressed. E-mail: ajhansen@zi.ku.dk

ined whether genetic records of paleocommunities might be preserved in sediments.

Small samples (2 g wet weight) were collected from disparate frozen and temperate sediment deposits: cores drilled into northeast Siberian permafrost stratigraphically dated from modern up to 1.5 to 2 Ma (million years) (*11*), and temperate New Zealand cave and coastal sediments dating from 0.6 to 3 ky (Table 1; table S1b) (*11*). The permafrost samples were obtained from one short tundra (bore) pit and seven cores (up to 31.1 m) drilled under carefully controlled conditions along a 1200-m stretch of the Arctic coast between the Lena and Kolyma rivers in former western Beringia (Table 1) (*11*). Contamination during the coring process was carefully monitored through the introduction of laboratory strains of *Serratia marcescens* bacteria around the drilling apparatus (*12*). The cores were stratigraphically characterized with radiocarbon accelerated mass spectrometry (AMS), magnetic- and biostratigraphic (pollen and paleontological) analyses (table S1a) (*11*), and samples removed from several positions to cover the entire Pleistocene record (Table 1). Each 2-g sample is thought to represent roughly the same amount of depositional activity, although conservative error margins on the older samples reflect stratigraphic imprecision. We obtained parallel samples ~0.5 km apart for the oldest layers and examined the variation in vegetative composition. All samples consisted of frozen soil with pore ice, with occasional fine rootlets (≤2 mm in diameter), seeds, and small unidentifiable multicellular fragments (Table 1) (*11*). Importantly, modern root growth does not penetrate below the active surface layer, so the inclusions represent the original flora. The New Zealand samples included dry silty sediment from a subalpine cave in the Clutha Valley, Otago, and sand from the interior and exterior of a bone of an extinct moa, *Euryapteryx curtus*, collected in situ from a coastal dune deposit in Northland (Table 1) (*11*).

DNA was extracted from the soil samples in independent specialist ancient DNA laboratories in Copenhagen and Oxford with previously established rigorous methods (*11*). Polymerase chain reaction (PCR) was used to amplify an ~130–base pair (bp) fragment of the chloroplast ribulose-bisphosphate carboxylase (*rbcL*) gene, and 100- to 280-bp fragments of the vertebrate mitochondrial 16*S*, 12*S*, cytochrome b (cyt b), and control-region genes. Positive *rbcL* amplifications were obtained from samples up to 300 to 400 ky old in both laboratories; in contrast, vertebrate mitochondrial amplifications could be obtained only up to 20 to 30 ky (Table 1). No amplification products could be obtained from the 1.5- to 2-Ma samples or from multiple controls (*1*, *11*, *13*). Sequences of the control *S. marcescens* bacteria were not detected. The PCR products were each cloned to examine taxonomic diversity, contamination, and the effects of damage artifacts (*1*, *10*, *13*, *14*). A total of 290 chloroplast and 91 mitochondria clones were sequenced. The short *rbc*L sequences allowed 274 of the chloroplast clones to be identified to the levels of class, order, or family in BLAST searches by identifying the highest taxonomic rank at which multiple GenBank sequences showed equal

Table 1. Sediment samples analyzed for plant chloroplast (*rbcL*) and vertebrate mitochondrial (16*S*, 12*S*, cyt b, control region) DNA. Core numbers, drilling year, depth (in meters below the surface), ice content (weight %), and carbon content (weight %) are given for the permafrost samples, along with the geographic locations and stratigraphic age of all samples. The number of clone sequences analyzed is indicated (excluding plant sequences containing frame-shift mutations and chimera sequences), along with the samples independently analyzed in Oxford. Russian stratigraphic nomenclature is given in (*11*). Taxonomic diversity is given by the number of clone sequences, assuming that those ≥96% identical represent a single taxon. Yr, years. An asterisk indicates samples containing visible rootlets. ND, no data, experiment not done.

Samples core/year/depth	Site	Age range (yr B.P.)	Ice con. (%)	C org. (%)	Indpt. replctn Oxford	No. of clones (*rbcL*/mtDNA)	Tax. divers. (*rbcL*)
		Permafrost					
Bore-pit 1/02/0.5	Kolyma lowland, Plakhin Jar (160°50′E, 68°40′N)	Seasonally frozen modern tundra soil	ND	ND	ND	38/ND	7*
1/93/4.0	Kolyma lowland, Kon'kovaya river (158°28′E, 69°23′N)	Holocene (*al*QIV) floodland (10.425 ± 45 yr)	30.0	1.3	y	32/14	7*
2/01/4.8	Laptev Sea coast, cape Bykovskii (129°30′E, 71°40′N)	Age of deposits—late Pleistocene (QIII) (18.980 ± 70 yr) permafrost age Holocene (QIV) (8–9 ky)	121.0	0.9	y	43/30	4
7/90/1.6	Kolyma lowland, Chukochia river (156°59′E, 69°29′N)	Late Pleistocene Icy Complex (*lal*QIII) (20–30 ky)	66.0	1.4 to 1.7	y	35/4	6
3/01/20.7	Laptev Sea coast, cape Svyatoi Nos (140°10′E, 72°55′N)	Middle Pleistocene Icy Complex (*lal*QII) (300–400 ky)	28.0	0.6	y	47/0	9
4/01/9.2	Laptev Sea coast, cape Svyatoi Nos (140°10′E, 72°55′N)	Middle Pleistocene Icy Complex (*lal*QII) (300–400 ky)	42.0	0.5	y	49/0	15
6/90/30.7	Kolyma lowland, Chukochia river (156°59′E, 69°29′N)	Late Pliocene early Pleistocene horizon (*lal*N2-QI) (1.5–2.0 Ma)	52.0	1.1	y	0/0	0*
6/90/31.1	Kolyma lowland, Chukochia river (156°59′E, 69°29′N)	Late Pliocene early Pleistocene horizon (*lal*N2-QI) (1.5–2.0 Ma)	30.0	1.4	ND	0/0	0*
		New Zealand					
Cave sediment	Clutha River (45°19′S, 169°20′E)	624 ± 50 yr	0.0	3.1	ND	36/30	29
Coast. sand ext. bone	Tokerau Beach (173°22′E, 34°53′S)	~1–3 ky	0.0	0.7	ND	ND/0	ND
Coast. sand int. bone	Tokerau Beach (173°22′E, 34°53′S)	~1–3 ky	0.0	ND	ND	ND/10	ND
Σ = 11					Σ = 6	Σ = 368	

highest similarity to the clones [allowing a maximum of 5 bp to be excluded in the comparison, modified from (*5*)]. Sequences containing frame-shift mutations were omitted to avoid possible nuclear copies (*15*). To allow for sequence heterogeneity (e.g., within-species variability and template damage), clones ≥96% identical were assumed to belong to the same taxon. Eleven classes (or subclasses), 23 orders, and 28 families of angiosperms (trees, shrubs, and herbs), gymnosperms (shrubs and trees), and mosses were identified in the samples (Table 2). All but three of the permafrost taxa have representatives in modern northeast Siberian tundra (*11*), although ~40% show differences from modern GenBank sequences. A bootstrap test confirmed that chloroplast sequences obtained from the geographically separate 300- to 400-ky samples, and those replicated in parallel at Copenhagen and Oxford (Table 1), represented the same underlying distributions (table S3) (*11*). This result suggests that the samples may be representative of vegetation over a relatively large area and is supported by analysis of the modern sample (0 ky), which contained sequences of all the angiosperms and mosses identified within at least 5 m of the sampling site. Importantly, the 300- to 400-ky sequences represent the oldest reproducible and authenticated ancient DNA to date. The New Zealand temperate cave sequences are more diverse than the permafrost sequences (Fig. 1A) and appear to be a close match for the inferred prehuman environment with a dominance of Podocarpaceae, Nothofagaceae, Malvaceae, Asterales, and Rubiaceae (*16*) (Table 2).

Table 2. Clones of chloroplast *rbcL* sequences identified to the level of class (or subclass), order, or family (see main text), with those ≥96% identical assumed to represent the same taxon. The number of genera yielding equal highest matches in BLAST searches is shown (in parentheses after taxon names), along with the maximum percentage similarities. Clone sequences that were independently replicated are in bold. *N*, number of samples analyzed. Taxa representing shrubs or trees (*), herbs (†), and mosses (‡) are indicated.

Sample age (ky B.P.)						Taxonomic identifications			
Cave	Permafrost								GenBank similarity (%)
0.6 *N* = 1	0 *N* = 1	10.4 *N* = 1	19 *N* = 1	20 to 30 *N* = 1	300 to 400 *N* = 2	Class or subclass (no. of genera)	Order (no. of genera)	Family (no. of genera)	
			Number of clones						
	1	7			**13**	Liliopsida	Poales	Cyperaceae (1 to 11)†	98 to 100
1		1	**8**	**4**	**34**			Poaceae (1 to 6)†	93 to 100
					3		Liliales	Liliaceae (3)†	100
1	2					Coniferopsida	Coniferales	Cupressaceae (1)*	92 to 93
15								Podocarpaceae (1 to 2)*	93 to 97
					1	Asteridae	Ericales (3)*		100
	12							Ericaceae (1 to 3)*	100
				1		Rosidae (22)			96
					1		Malpighiales (4)*		96 to 98
	5	**15**	**16**	**10**	**12**			Salicaceae (1 to 4)*	97 to 100
			1					Flacourtiaceae (1)*	97
1							Myrtales	Onagraceae (1)	90
1							Malvales	Malvaceae (28)	95
	4						Fagales (4 to 6)*		98 to 100
2								Nothofagaceae (1)*	96 to 97
1							Fabales	Fabaceae (1)	92
			1	1	1		Rosales (2 to 5)		87 to 96
			1					Rhamnaceae (1)*	96
			15	**9**	**4**			Rosaceae (1 to 3)†	94 to 97
					1			Moraceae (1)*	98
		1			**5**		Brassicales	Brassicaceae (1 to 2)†	98 to 100
			1		3	Caryophyllidae	Caryophyllales (4 to 5)		100
		2						Caryophyllacae(1)†	97
5						Caryophyllidae	Caryophyllales	Polygonaceae (2 to 4)	93 to 98
					2	Asteridae (10)			97 to 100
				1	1		Lamiales (3)		100
		2		1				Antirrhinaceae (1)†	98 to 100
1							Asterales (11)		87
		4		**7**	**9**			Asteraceae (1 to 7)†	98 to 100
				1				Campanulaceae(1)†	100
1							Gentianales	Rubiaceae (1)*	95
					2	Eudicotyledon	Ranunculales	Papaveraceae (1)†	100
	4					Bryidae (2)‡			98 to 100
	8						Rhizogoniales	Rhizogoniaceae(1)‡	97
					1		Hypnales	Hylocomiaceae(1)‡	100
					2		Bryales (2)‡		98
	1					Polytrichopsida	Polytrichales	Polytrichaceae (1)‡	93
1						Bryopsida (3)‡			96
1							Grimmiales	Grimmiaceae (1)‡	93
1							Pottiales	Pottiaceae (1)‡	95
Σ = 32	Σ = 37	Σ = 32	Σ = 43	Σ = 35	Σ = 95	Σ = 11	Σ = 23	Σ = 28	

We identified vertebrate mitochondrial sequences by BLAST analysis and constructed phylogenetic trees (*11*) using GenBank taxa with the highest scores, as well as outgroups. Eight different extinct and extant taxa were detected in the permafrost samples: woolly mammoth, steppe bison, horse, reindeer, musk ox, brown lemming, hare, and an unidentified bovid related to the musk ox (Table 3; figs. S1 to S3) (*11*). Mammoth sequences were obtained for two different regions of cyt b and one of 16*S* (Table 3; figs. S1 to S3) (*11*). In New Zealand, the coastal sand samples were negative, although sand from the interior of the in situ bone yielded *E. curtus* sequences (Table 3; fig. S4A) (*11*). In contrast, the cave sample yielded 12*S* and control region sequences of two extinct moa taxa (*Megalapteryx didinus* and *Pachyornis elephantopus*) and avian species currently absent from the area (*Cyanoramphus* spp.) (Table 3; fig. S4, A and B). Three of the moa clone sequences appeared to represent recombination products and were probably artifacts created during PCR (*10*, *13*). It is interesting that such sequence variation characteristic of damage-related artifacts (*10*, *13*) was observed in the temperate samples but appeared minimal in the permafrost samples—for example, only 3 of 11 substitutions in mammoth cyt b sequences resulted in amino acid replacements (table S4) (*11*). Furthermore, the domination of large herbivore sequences in both the permafrost and cave sediments indicates that a major source may be high-volume waste products (feces and urine).

The presence of multiple extinct taxa strongly supports the authenticity of the data, whereas the dramatically different taxonomic

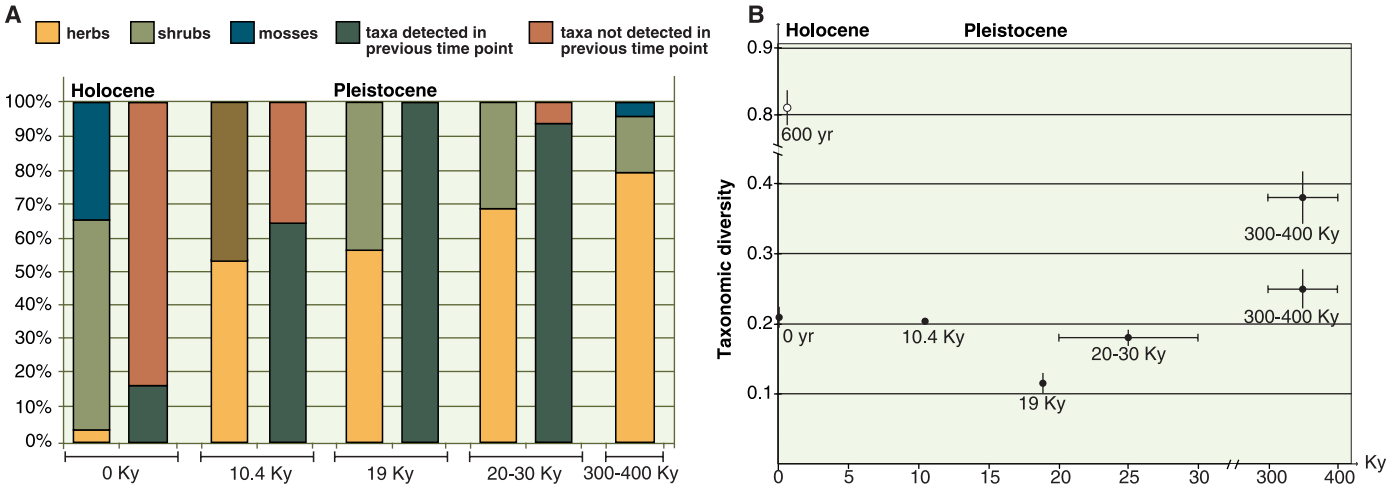

Fig. 1. Change in plant composition and diversity through time in permafrost core samples. (**A**) For each time period, the proportion of shrubs, herbs, and mosses observed is indicated, along with the proportion of all taxa that are detected or not detected in samples from the previous time point. Clone sequences ≥96% identical are assumed to represent one taxon. (**B**) Changes in taxonomic diversity through time, as measured by the number of sequence groups (clone sequences with <96% similarity) divided by the total number of clone sequences obtained for that sample. To standardize the number of clones sequenced, sequence diversity was measured in each sample with 1000 data sets of 32 (the smallest data set, Table 1) randomly chosen clones. Black dots represent permafrost samples; white dots represent New Zealand cave samples.

Table 3. Vertebrate mitochondrial sequences identified in Siberian and New Zealand samples through phylogenetic analysis (*11*) (figs. S1 to S4). The number, length, and genetic location of clone sequences are given, along with the closest match (%) among living and extinct (†) taxa found in GenBank. Reference sequences of moa and bison taxa determined in Oxford (*), and musk ox and lemming determined in Copenhagen (‡), are shown. Reference parrot sequences (*29*). Clone sequences in bold were independently obtained in Oxford.

Sample age (ky B.P.)					Region (mtDNA)	Sequence length (bp)	Taxonomic identifications	
New Zealand		Siberia						
Cave 0.6	Bone 1 to 3	10.4	19	20 to 30			Taxa with highest sequence similarity	Seq. similarity (%)
		1		2	cyt b	98	*Mammuthus primigenius* (mammoth)†	98 to 99
			7		cyt b	229	*Mammuthus primigenius* (mammoth)†	99 to 100
		8	**4**	1	16*S*	92 to 93	*Mammuthus primigenius* (mammoth)†	97 to 100
			12		16*S*	90	*Equus caballus* (horse)	98 to 100
			4		16*S*	88 to 90	*Lemus lemus* (lemming)	97‡
		2			16*S*	95	*Lepus europaeus* (hare)	96
		2	1	1	Control region	124 to 125	*Bison* spp. (bison)†	98 to 100*
			1		16*S*	93	*Ovibos moschatus* (musk ox)	100
			1		Control region	129	*Ovibos moschatus* (musk ox)	82‡
		1			Control region	124	*Rangifer tarandus* (reindeer)	98
15					Control region	202 to 203	*Megalapteryx didinus* (Upland moa)†	97 to 100*
2					Control region	204	*Pachyornis elephantopus* (Heavy-footed moa)†	99*
	10				Control region	202 to 203	*Euryapteryx curtus* (Coastal moa)†	96 to 100*
11					12*S*	228 to 230	*Megalapteryx didinus* (Upland moa)†	97 to 100
2					12*S*	234	*Cyanoramphus novaezeelandiae* (New Zealand Parakeet)	98 (*29*)
Σ = 30	Σ = 10	Σ = 14	Σ = 30	Σ = 4				

composition down the length of the permafrost cores indicates stratigraphic integrity. This demonstrates that sedimentary genetic signals of plant and animal communities can be preserved for considerable periods in both permafrost and temperate conditions. Furthermore, chloroplast sequences are essentially absent from angiosperm pollen (*15*, *17*), which implies that most of the plant sequences originate from locally deposited seeds, or somatic tissue such as the observed fine rootlets that are abundant in most soils and can spread up to 10 m horizontally (*18*, *19*). Consequently, sedimentary DNA provides a unique opportunity to assess the accuracy of pollen-based paleoenvironmental records, which can be limited in distribution and are complicated by taxon-specific variation in vegetative reproduction, pollen productivity, and dispersal ability (*20*, *21*).

The utility of sedimentary records is apparent from the views of mid- to late Pleistocene Beringian paleoecology revealed by just six permafrost samples. For example, the Beringian vegetation around the last glacial maximum (LGM), 22 to 16 ky, has variously been suggested to be a sparse and poorly productive polar desert unable to support a diverse megafauna; a dense herb-dominated steppe/tundra supporting populations of bison, horse, and mammoth; or a mosaic of different tundra types (*20*, *22*–*27*). The diverse and abundant sequences of herbs (e.g., Asteraceae, Poaceae, Antirrhinaceae, Campanulaceae, and Rosaceae) and mammals around the peak of the LGM clearly indicate a herb-dominated community with populations of bison, horse, musk ox, and mammoth (*20*, *22*, *27*). Perhaps the most surprising trend in the data is the apparent decline in the ratio of herbs to shrubs throughout the Pleistocene, which dramatically accelerates in the Holocene (Fig. 1A). Furthermore, after the LGM, the true grasses (Poaceae) appear to decline markedly at the expense of sedges (Cyperaceae) (Table 2), which may be connected with the late Pleistocene megafaunal extinctions (*20*, *23*). Overall, the data show a decreased floral taxonomic diversity at the peak of the LGM, followed by an increase toward the Holocene boundary and a dramatic change in composition during the Holocene (Table 2 and Fig. 1, A and B).

If vertebrate and plant genetic signals can be routinely retrieved from other sedimentary deposits, and can be correlated with stratigraphic position over long time periods, it will have major implications for many fields, including paleoecology, archaeology, and paleontology. For example, archaeological investigations could use core samples to link occupation layers with genetic groups, avoiding the current limitations imposed by destructive sampling and the pervasive modern human DNA contamination of excavated material (*6*, *10*, *28*).

References and Notes

1. A. Cooper, H. N. Poinar, *Science* **289**, 1139 (2000).
2. M. Krings *et al.*, *Cell* **90**, 19 (1997).
3. I. Barnes, P. Matheus, B. Shapiro, D. Jensen, A. Cooper, *Science* **295**, 2267 (2001).
4. A. Cooper *et al.*, *Nature* **409**, 704 (2001).
5. H. N. Poinar *et al.*, *Science* **281**, 402 (1998).
6. P. Endicott *et al.*, *Am. J. Hum. Genet.* **72**, 178 (2003).
7. J. R. Stewart, A. Lister, *Trends Ecol. Evol.* **16**, 608 (2001).
8. L. P. Waits, S. L. Talbot, R. H. Ward, G. F. Shields, *Conserv. Biol.* **12**, 408 (1998).
9. M. Richards *et al.*, *Am. J. Hum. Genet.* **59**, 185 (1996).
10. M. T. P. Gilbert *et al.*, *Am. J. Hum. Genet.* **72**, 32 (2003).
11. Supporting material is available at *Science* Online.
12. E. Willerslev, A. J. Hansen, H. Poinar, in preparation.
13. E. Willerslev, A. J. Hansen, B. Christensen, J. P. Steffensen, P. Arctander, *Proc. Natl. Acad. Sci. U.S.A.* **96**, 8017 (1999).
14. A. J. Hansen, E. Willerslev, C. Wiuf, T. Mourier, P. Arctander, *Mol. Biol. Evol.* **18**, 262 (2001).
15. J. L. Blanchard, G. W. Schmidt, *J. Mol. Evol.* **41**, 397 (1995).
16. M. McGlone, *N.Z. J. Ecol.* **25**, 1 (2001).
17. C. W. Birky Jr., *Proc. Natl. Acad. Sci. U.S.A.* **92**, 11331 (1995).
18. R. B. Jackson, H. A. Mooney, E.-D. Schulze, *Proc. Natl. Acad. Sci. U.S.A.* **94**, 7362 (1997).
19. T. A. Volk, L. P. Abrahamson, E. H. White, *Root Dynamics in Willow Biomass Crops* (SUNY College of Environmental Science and Forestry, Syracuse, NY, 2001).
20. R. D. Guthrie, *Frozen Fauna of the Mammoth Steppe: The Story of Blue Babe* (Univ. of Chicago Press, Chicago, IL, 1990).
21. P. M. Anderson, P. J. Bartlein, L. B. Brubaker, *Quat. Res.* **41**, 306 (1994).
22. M. Hopkins, J. V. Matthews Jr., C. E. Schweger, S. B. Young, Eds., *Paleoecology of Beringia* (Academic Press, New York, 1982).
23. L. C. Cwynar, J. C. Ritchie, *Science* **208**, 1375 (1980).
24. P. A. Colinvaux, F. H. West, *Quart. Rev. Archaeol.* **5**, 10 (1984).
25. P. A. Colinvaux, *Nature* **382**, 21 (1996).
26. V. G. Goetcheus, H. H. Birks, *Quat. Sci. Rev.* **20**, 135 (2001).
27. B. A. Yurtsev, *Quat. Sci. Rev.* **20**, 165 (2001).
28. M. Hofreiter, D. Serre, H. N. Poinar, M. Kuch, S. Pääbo, *Nature Rev. Genet.* **2**, 353 (2001).

29. A. Cooper, unpublished data. See (*11*) sample information for details.

30. We thank R. Holdaway, T. Worthy, and A. Tennyson (Te Papa Tongarewa Museum of New Zealand) for sequences and samples from New Zealand, and A. Sher, I. Barnes, K. Raundrup, T. B. Berg, M. Andersen, B. Jensen, and I. Jensen for contemporary and ancient Arctic samples. The manuscript benefited from discussion with the above and A. Currant, T. Higham, K. Aaris-Sørensen, R. Rønn, B. Christensen, B. Vest Pedersen, P. Arctander, H. Siegismund, O. Humlum, P. Hartvig, O. Seberg, S. Jonasson, M. B. Hebsgaard, T. Mourier, S. Mathiasen, A. Drummond, D. Froese, G. Zazula, P. Matheus, and C. Schweger. A.C. thanks Victoria University of Wellington, G. Chambers, and P. Baverstock for helpful assistance with the parrot phylogenetic research. We thank V. Kiel and J. Andersen for technical support in the building of Copenhagen clean lab facilities, and the Oxford University Museum of Natural History for providing laboratory facilities in Oxford. E.W., A.J.H., J.B., and T.B.B. were supported by the Villum Kann Rasmussen Fonden, Denmark. A.C., M.T.P.G., B.S., and M.B. were supported by the UK National Environmental Research Council and the Wellcome Trust, and B.S. was supported by the Rhodes Trust. C.W. was supported by the Carlsberg Foundation and the Medical Research Council, UK. D.A.G. was supported by the Russian Foundation for Basic Research, grant 01-05-65043.

Supporting Online Material

www.sciencemag.org/cgi/content/full/1084114/DC1
Materials and Methods
Figs. S1 to S4
Tables S1 to S4
References

4 March 2003; accepted 2 April 2003
Published online 17 April 2003;
10.1126/science.1084114
Include this information when citing this paper.

Activation of Integrin αIIbβ3 by Modulation of Transmembrane Helix Associations

Renhao Li,[1] Neal Mitra,[2] Holly Gratkowski,[1] Gaston Vilaire,[2] Rustem Litvinov,[3] Chandrasekaran Nagasami,[3] John W. Weisel,[3] James D. Lear,[1] William F. DeGrado,[1]* Joel S. Bennett[2]*

Transmembrane helices of integrin α and β subunits have been implicated in the regulation of integrin activity. Two mutations, glycine-708 to asparagine-708 (G708N) and methionine-701 to asparagine-701, in the transmembrane helix of the β3 subunit enabled integrin αIIbβ3 to constitutively bind soluble fibrinogen. Further characterization of the G708N mutant revealed that it induced αIIbβ3 clustering and constitutive phosphorylation of focal adhesion kinase. This mutation also enhanced the tendency of the transmembrane helix to form homotrimers. These results suggest that homomeric associations involving transmembrane domains provide a driving force for integrin activation. They also suggest a structural basis for the coincidence of integrin activation and clustering.

The mechanism regulating the activation state of integrins is emerging from structural investigations (*1*, *2*). Electron microscopy of several integrins and crystallography of αvβ3 (*3*–*5*) indicate that integrins are composed of a globular ligand-binding head and two flexible rodlike stalks containing the carboxyl-terminal portions of the integrin α and β